

High-Precision Overlay Registration via Spatial-Terminal Iterative Learning in Roll-to-Roll Manufacturing

Zifeng Wang, Xiaoning Jin, *Member, IEEE*,

Abstract—Roll-to-roll (R2R) printing technologies are promising for high-volume continuous production of substrate-based electronic products. One of the major challenges in R2R flexible electronics printing is achieving tight alignment tolerances, as specified by the device resolution (usually at the micro-meter level), for multi-layer printed electronics. The alignment of the printed patterns in different layers is known as registration. Conventional registration control methods rely on real-time feedback controllers, such as PID control, to regulate the web tension and the web speed. However, those methods may lose effectiveness in compensating for recurring disturbances and supporting effective mitigation of registration errors. In this paper, we propose a Spatial-Terminal Iterative Learning Control (STILC) method integrated with PID control to iteratively learn and reduce registration error cycle-by-cycle, converging it to zero. This approach enables unprecedented precision in the creation, integration, and manipulation of multi-layer microstructures in R2R processes. We theoretically prove the convergence of the proposed STILC-PID hybrid approach and validate its effectiveness through a simulated registration error scenario caused by axis mismatch between roller and motor, a common issue in R2R systems. The results demonstrate that the STILC-PID hybrid control method can fully eliminate the registration error after a feasible number of iterations. Additionally, we analyze the impact of different learning gains on the convergence performance of STILC.

Index Terms—Iterative learning control (ILC), advanced manufacturing, roll-to-roll (R2R) printing process, registration error.

I. INTRODUCTION

ROLL-TO-ROLL (R2R) printing systems offer a promising approach for high-throughput and continuous manufacturing of substrate-based products, such as thin-film printing electronic devices, batteries, and organic photovoltaics [1]–[5]. Roll-to-roll processing shows promising industrial scalability for next-generation energy technologies, enabling continuous mass production of both polymer-based energy storage materials and perovskite solar devices [6], [7]. However, the inter-layer misalignment issue in multi-layer printing processes using R2R printing systems remains a critical challenge in applications. Registration Error (RE), defined as the misalignment of printed patterns across different layers, must be controlled within a tight tolerance to ensure the

functionality of multi-layer products manufactured by R2R printing systems. This is essentially a challenging control task to control the positioning behavior of a flexible and lightweight *substrate*, referred to as *web* in R2R processes.

While RE can occur in both the longitudinal and lateral directions of the web, longitudinal errors often present the greatest control challenges, which is the primary focus of this work [8]. In the following discussion, RE specifically refers to longitudinal registration error. RE is primarily caused by fluctuations in web tensions and web speeds [9]–[11]. Due to the bendable and stretchable nature of the substrate (polymer films such as PET and PEN) handled by R2R printing systems, fluctuations in web tension and web speed are often inevitable. Additionally, even small disturbances or uncertainties in the system can result in significant fluctuations due to the low inertia of the web. These challenges in controlling RE limit the applicability of R2R printing processes for many emerging flexible electronics technologies in industrial practice.

Several studies have focused on designing feedback controllers to regulate web tensions and mitigate registration errors. [12] presented a robust linear parameter-varying model predictive control (LPV-MPC) scheme that enhances tension tracking performance by addressing disturbances caused by model uncertainties and slowly-changing dynamics. [13] proposed a data-driven model predictive control (DD-MPC) method that minimizes multistage registration errors by obtaining the plant model from sensor data and handling multi-input and multi-output systems. In [14], a decentralized controller for web processing lines achieves exponential convergence of web tension and transport velocity variations by dividing the system into tension zones and computing equilibrium inputs and reference velocities. A model-based speed variation compensation PD control method has also been developed to eliminate disturbances caused by tension variation during the speed-up phase [15]. Furthermore, a fully decoupled proportional-derivative (FDPD) control algorithm was proposed to remove couplings between upstream register control and downstream registration errors, controlling multiple printing units and accommodating different web lengths between adjacent gravure cylinders [9].

Compared to the aforementioned feedback control methods, feedforward control approaches can provide better system stability when tackling transient disturbances, which is critical when controlling flexible and lightweight objects such as the web in R2R systems. Feedforward controllers generate compensation signals based on their internal settings without

This work was supported in part by the National Science Foundation under Grants CMMI-1943801 and CMMI-1907250. (*Corresponding author: Xiaoning Jin.*)

The authors are with the Department of Mechanical and Industrial Engineering, Northeastern University, Boston, MA 02115 USA (email: wang.zifen@northeastern.edu; xi.jin@northeastern.edu).

waiting for the occurrence of output errors. Moreover, angle-periodic disturbances commonly occur in R2R systems, largely due to the rotational nature of multiple rollers involved in the process. To address these disturbances, researchers have been exploring the use of iterative learning control (ILC), as a type of feedforward control methods for improving web tension control in R2R processes.

Iterative learning control (ILC) is a class of feedforward control methods specifically designed for repetitive manufacturing processes [16]. ILC generates a complete control input profile for the upcoming operation cycle based on the input and output data from previous iterations. In earlier studies [17], [18], Norm Optimal ILC (NOILC) methods have been designed to mitigate transient behaviors in R2R processes by iteratively regulating web tensions. NOILC methods have demonstrated superior performance in tracking reference web tension profiles. However, there are two limitations to the broader application of this paradigm in practice:

(1) NOILC requires an accurate nominal model of the controlled R2R system to estimate the tension tracking error in an iteration. However, a satisfactory nominal model is not always accessible in industrial applications, as R2R systems and flexible webs can involve high nonlinearities and uncertainties.

(2) The control goal is set to strictly track a preset tension profile. In practice, applications often allow for slight deviations in tensions throughout the cycle, while focusing on closely monitoring the RE, which is the *terminal output* (i.e., the measurable output at the end of each operation cycle). Continuously tracking a preset tension profile can be challenging and may underutilize the allowable tolerance range, resulting in slow convergence and high computational burden.

To overcome these two limitations of applying ILC in R2R registration control, we propose a Terminal ILC (TILC) framework that utilizes only the terminal measurement of RE from the previous iteration, rather than a tension profile, to update the control input profile. In a multi-layer printing process, the RE can only be measured after the downstream pattern has been printed [19]–[21], and the printing of the downstream pattern typically signifies at the end of an operation cycle. Therefore, TILC is a suitable framework for R2R RE control tasks. To eliminate the need for accurate nominal models, we are inspired by earlier ILC research where the simple but effective P-type ILC updating law was prevalent [22], [23]. The P-type ILC updating law can be effectively incorporated into the TILC framework with a predefined basis function. The ideal basis function is designed to provide an input signal profile that compensates for the disturbance in an exactly opposite manner. However, if the basis function deviates significantly from the desired profile, the TILC method may suffer from instabilities, slower convergence, or even failure. Therefore, constructing an appropriate basis function for TILC is crucial to achieving optimal control performance. For instance, a previous study [24] employed constant-value basis functions to simplify controller design. That is, the control input remains constant during each iteration, changing only between iterations. However, any system behaviors inside an iteration

were ignored, which could have been captured by leveraging prior system knowledge reasonably. Other approaches have designed basis functions based on a state-space model of a Rapid Thermal Processing Chemical Vapor Deposition (RT-PCVD) system [25] or used data-driven techniques such as iterative dynamical linearization [26]–[28] and neural network-based methods [24]. However, these approaches still rely on nominal models identified from online process data, which can be computationally expensive or technically challenging for industrial users.

In this study, we propose a streamlined and effective method for designing TILC controllers to mitigate RE in R2R printing processes, while minimizing hardware computation demand. Observing that perfect tension tracking of the reference profile is not required to achieve zero final RE measurement, we hypothesize that multiple control input profiles, each approximating the reference, can still result in zero RE by the end of the iteration. A P-type TILC updating law can converge to one of these control input profiles, iteratively guaranteeing that the RE approaches zero. Consequently, the basis function can be designed solely by observing tension fluctuations, eliminating the need for prior knowledge or system identification of the R2R system. Our previous work [29] has demonstrated the effectiveness of this approach through simulation. In this paper, we further analyze the convergence conditions theoretically and provide clear guidance for practitioners in designing the TILC controller.

To further ensure the effectiveness of the basis function design for R2R registration control, we leverage the insight that rollers in R2R systems are components of rotary machinery, which typically exhibits spatial (angular) periodicity. Disturbances in rotary machine systems, including components like spindles in lathing, milling, and grinding processes, frequently show a dependency on angular displacements, reflecting the circular nature of these systems [30]. To tackle the angularly periodicity in these repetitive processes, ILC frameworks have been adapted to Spatial Iterative Learning Control (SILC), which employs an angular index for iteration steps, shifting focus from the traditional time-dependent iteration approach. The SILC methods have been successfully demonstrated in various applications such as additive manufacturing, wind turbines, and robotics. In particular, Afkhami *et al.* designed a SILC method to adjust the voltage pulse width of electrohydrodynamic jet (e-jet) printing processes in a 2D spatial domain based on the layer-wise repeated nature of e-jet printing processes [31]–[33]. Liu *et al.* investigated a PD-type SILC for enhancing wind turbine efficiency by adjusting the pitch angle to maintain consistent output power at higher wind speeds, considering that the wind turbine system is spatially periodic in terms of angular displacement [34]. Yang *et al.* presented a SILC method enabling a robot to learn desired paths in unknown environments with fixed spatial constraints by updating its trajectory based on interaction forces that are not periodic in time [35]. High-speed trains, with their space-dependent parameters and uncertainties, are another typical class of applications for SILC. It aims to enhance train performance, particularly in terms of tracking speed profiles in the spatial domain [36]–[40]. Kim *et al.* introduced a backlash

control algorithm using TILC to mitigate backlash impact in vehicle systems through angle domain control [41]. They designed ILC in the angle domain with access only to the terminal output for a spatial period, which was similar to the strategy we apply to R2R printing processes in this work.

In this work, we focus on the application of SILC to R2R printing processes. The preliminary results [29] of the present study specifically designed a cosine-form basis function in the spatial domain. This spatially-dependent basis function forms the foundation for our proposed method named Spatial-Terminal Iterative Learning Control (STILC). By integrating STILC with a decentralized PID controller [14], we aim to achieve effective registration control in R2R printing systems. This approach leverages the advantages of SILC and the well-established decentralized PID control scheme, offering promising prospects for enhancing registration control in R2R printing applications. Building upon our foundational methods and insights presented in [29], we now demonstrate the convergence condition of STILC and provide reliable guidance of STILC design through rigorous analysis. Our main contributions are outlined as follows:

(1) A model-free ILC framework, STILC, is proposed to effectively mitigate RE in R2R printing processes for manufacturing multi-layer structures on flexible substrates in a continuous manner. Compared to model-based NOILC methods for tension profile tracking control, our work provides an alternative approach to designing ILC controllers for mitigating RE in R2R printing processes, reducing reliance on expert knowledge and minimizing hardware computation demands.

(2) With a predefined basis function, the proposed STILC can update the control input profile for an iteration by adjusting only one parameter based on the terminal RE measurement. This feature significantly reduces the computational burden of obtaining the control input profile as a high-dimensional vector.

(3) We provide criteria for designing the basis function and learning gain in the proposed controller to effectively reduce registration errors. These criteria enable practitioners to design a basis function by approximating the tension fluctuation profile and subsequently choose an appropriate learning gain for an effective STILC. This efficient approach to controller design broadens the applicability of STILC across a wider range of repetitive manufacturing processes governed by linear time-varying (LTV) dynamics.

The remainder of this paper is organized as follows: Section II reviews the physics-based model of the R2R registration error using the perturbation-based approximation method. In Section III, the STILC-PID hybrid controller is designed, followed by the convergence analysis. Section IV demonstrates its performance in terms of registration error control effectiveness and speed of convergence by experimenting with different system parameters in simulations. Section V concludes the paper.

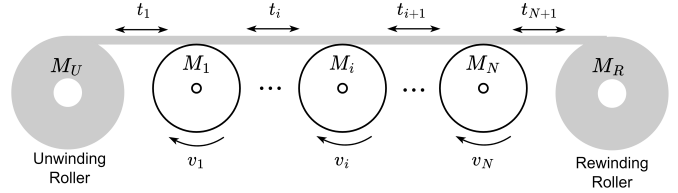


Fig. 1: A General R2R Printing System with Unwind, rewind, and Intermediate Rollers

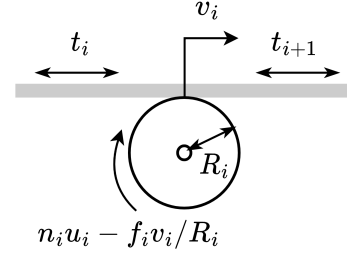


Fig. 2: Dynamics of One Intermediate Roller

II. R2R REGISTRATION ERROR DYNAMICS AND DISTURBANCES MODELING

A. R2R Registration Error Dynamics

A typical R2R printing system comprises a web handling system that transports the flexible web (substrate) through a series of rollers. In our preliminary work [29], we particularly studied an R2R printing system with gravure printing rollers, which represents a prevalent configuration of R2R systems in flexible-substrate electronics manufacturing processes. Figure 1 illustrates such an R2R system with one unwinding roller (M_U), one rewinding roller (M_R), and N intermediate rollers (M_1 to M_N).

We make the following two assumptions on the system:

Assumption 1: There is no slippage between the roller and the web [11], [14]. In other words, the tangential roller speeds ($v_i, i = 1, 2, \dots, N$) are equal to the speeds of the following web span. The web span is defined as the web section between two successive rollers.

Assumption 2: The web tension $t_i, i \in \{1, 2, \dots, N + 1\}$ and web speed $v_i, i \in \{1, 2, \dots, N\}$ are uniformly distributed through a span.

The dynamics of a single motorized intermediate roller in Fig. 2 are described by the following differential equation, considering the mechanics of the rotational system [14]:

$$\frac{J_i}{R_i} \dot{v}_i = (t_{i+1} - t_i)R_i + n_i u_i - \frac{f_i}{R_i} v_i \quad (1)$$

where J_i , R_i , n_i , and f_i are the inertia, radius, gearing ratio, and friction coefficient of roller i , respectively. u_i is the torque input provided by the motor of roller i . $i \in \{1, 2, \dots, N\}$ is the index of the roller. It describes how the web behaves according to the controlled motor torque and the inner friction effect.

Some of the intermediate rollers can be assigned to work as printing rollers. In this paper, the RE is defined as the intended overlay position of a pattern and the actual position printed by

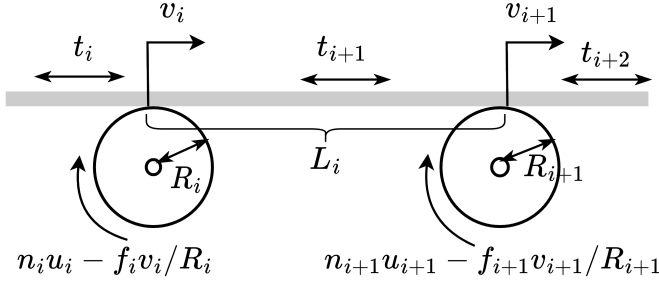


Fig. 3: Dynamics of a Two-Roller Printing Unit

two consecutive printing rollers. Thus, we extend the one roller dynamic model in Fig. 2 to the two-roller printing rollers, as shown in Fig. 3.

For a two-roller system, we can derive the dynamic equations for v_i and v_{i+1} , and the dynamic equations for the tension through the web span between these two rollers [14]. The dynamic equations for the tension are

$$L_i \dot{t}_i = AE(v_i - v_{i-1}) + t_{i-1}v_{i-1} - t_i v_i \quad (2)$$

where L_i is the span length, A is the cross-sectional area of the substrate, E is the elastic modulus of the substrate. This equation is derived using the mass conservation principle, which means the mass of the web flowing out of the upstream section is equal to the mass flowing into the downstream section. The details can be found in [42].

To eliminate the nonlinear terms in Eq. (2), the perturbation method is used to linearize the equation [14]. We define the following perturbation variables:

$$\begin{aligned} v_i(\tau) &= v_i^r + V_i(\tau) \\ t_i(\tau) &= t_i^r + T_i(\tau) \\ u_i(\tau) &= u_i^r + U_i(\tau) \end{aligned} \quad (3)$$

where τ denotes time. v_i^r and t_i^r are speed and tension references. V_i and T_i are the variations (perturbation variables) in speed and tension. u_i^r is the equilibrium control input to maintain the speed and tension at the given reference levels. u_i^r can be calculated as follows:

$$u_i^r = \frac{f_i}{n_i R_i} v_i^r - \frac{R_i}{n_i} (t_{i+1}^r - t_i^r) \quad (4)$$

Then we can obtain the dynamic equations for the two-roller case in perturbation form:

$$\begin{cases} \frac{J_j}{R_j} \dot{V}_j = (T_{j+1} - T_j)R_j + n_j U_j - \frac{f_j}{R_j} V_j & j = i, i+1, \\ L_k \dot{T}_k = AE(V_k - V_{k-1}) \\ + (t_{k-1}^r V_{k-1} + v_{k-1}^r T_{k-1}) - (t_k^r V_k + v_k^r T_k) \\ + (t_{k-1}^r v_{k-1}^r - t_k^r v_k^r) & k = i, i+1, \\ & i+2 \end{cases} \quad (5)$$

Note that Eq. (5) includes state variables v_{i-1} and t_{i-1} that are not shown in Fig. 3 but exist in Fig. 1. To simplify

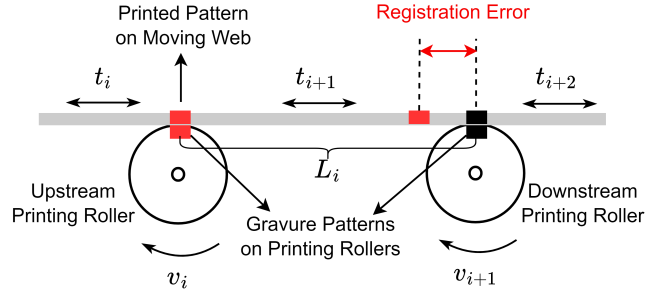


Fig. 4: Registration Error in A Two-Roller Printing Unit (The compression rollers are hidden)

the control problem formulation, we assume that in an R2R system shown in Fig. 1, tensions and speeds of the rollers except for the printing rollers M_i and M_{i+1} are well-controlled and always equal to the reference values. Therefore, the whole system can be described by Eq. (5) with the five state variables $(V_i, V_{i+1}, T_i, T_{i+1}, T_{i+2})$. Therefore, in modeling general R2R systems, as shown in Fig. 1, we focus exclusively on the two-roller section illustrated in Fig. 3.

After obtaining the state space equations in Eq. (5) describing tension and speed variations in the two-roller system, we now designate the two rollers as two adjacent gravure printing rollers and present the dynamic model of the R2R registration error. Figure 4 shows the schematic of two adjacent gravure printing rollers. The red squares represent the patterns printed by the upstream roller. The black square represents the pattern printed by the downstream roller. The registration error is defined as the distance between the two patterns printed by the upstream roller and the downstream roller respectively. Without loss of generality, we make the following assumption on the span length.

Assumption 3: The span length between the two printing rollers is equal to the circumference of the upstream roller. ($L_i = 2\pi R_i$)

By Assumption 3, we know that when the substrate is running with steady tension and speed, the pattern printed by the downstream roller (black square) should coincide with the pattern printed previously by the upstream roller (red square). Fluctuations in tension and speed due to internal or external disturbances can cause the misalignment between consecutive printed patterns, resulting in registration errors.

Based on [11], the registration error is given as the following differential equation, which describes the linearized dynamic model of the RE changing rate and the tension and speed variations:

$$\dot{r}_i(\tau) = \frac{1}{AE} [v_i^r T_i(\tau - \tau_j^r) - v_{i+1}^r T_{i+1}(\tau)] \quad (6)$$

where r_i is the registration error generated by printing roller i and printing roller $i+1$, τ_j^r is the reference time interval for the upstream printed pattern to be transported to the downstream roller in the j^{th} iteration. Since the variations of tension and speed are relatively small, the actual time interval in each iteration should be very close to a constant value τ^r . Thus, τ^r is used as the approximated time interval in [11]. In

the next section, we will make use of this approximation to rewrite Eq. (6) in the iteration domain.

Under Assumptions 1-3, Equations (5) and (6) describe the state-space model of the R2R registration error problem as a linear system. The input variables U_i and U_{i+1} are the motor torque variations of the two printing rollers. The output variable is the registration error. The state variables are the variations of the speeds (V_i, V_{i+1}) and tensions (T_i, T_{i+1}).

Remark 1: The process of generating the registration error is repetitive. Each time the pattern is printed, the last operation cycle is terminated and a new operation cycle starts. This is why ILC is considered a suitable approach for such repetitive processes.

Remark 2: It should be noted that even though r_i is the variable representing registration error, the actual registration error is only generated every time the downstream pattern is printed. Therefore, the registration error is only measured every time the printing roller completes a cycle. During the cycle, there is no continuous measurement of the registration error. This is the reason for us to design the terminal ILC method for R2R registration control.

B. Modeling of Cycle-Induced Repetitive Disturbances

From Eq. (6), we know $r(\tau) \equiv 0$ if $T(\tau) \equiv 0$ and $V(\tau) \equiv 0$. However, inherent and exterior disturbances make it difficult to always maintain steady tensions and speeds in an R2R system. In this paper, an axis mismatch is introduced to the upstream roller in the two-roller system in Fig. 4. Axis mismatch phenomena commonly occur between the motor shaft and the geometric center of the roller, which causes an angle-periodic disturbance for the repetitive rotary process [30].

When the mismatch exists, the effect of this eccentric printing roller is equivalent to a roller with its radius varying over the phase angle. We define the angle-varying radius as the equivalent radius of the roller with respect to the phase angle. Therefore, the parameter R_i is transferred to a function of the phase angle:

$$R_i(\theta_i) = R_i^r + e \cos(\theta_i) \quad (7)$$

where R_i^r is the constant value of the original radius when there is no axis mismatch, e is the eccentricity defined as the distance between the motor shaft and the roller center. Figure 5 shows how the equivalent radius R_i varies with respect to the phase angle through an operation cycle.

The axis mismatch introduced to the upstream roller will result in two changes in the previous two-roller system: (1) The linear time-invariant (LTI) system becomes a linear time-varying (LTV) system due to the varying parameter R_i . (2) The equilibrium control input u_i^r is no longer a constant value but an angle-varying function as shown in Eq. (8).

$$u_i^r = \frac{f_i}{n_i R_i(\theta_i(\tau))} v_i^r - \frac{R_i(\theta_i(\tau))}{n_i} (t_{i+1}^r - t_i^r) \quad (8)$$

Assumption 4: Web tensions and speeds are detectable in real-time, and the registration error of each printing cycle can only be detected at the end of each cycle.

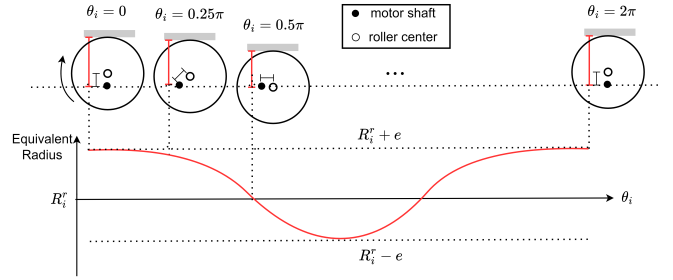


Fig. 5: Phase-Angle-Varying Equivalent Radius Caused by Axis Mismatch

Under Assumptions 1-4, the goal of the following controller design is to minimize the registration error by adjusting the motor torque inputs u_i and u_{i+1} .

III. CONTROLLER DESIGN AND ANALYSIS

A. STILC-PID Hybrid Controller Design

The controlled system in Sec. II is an LTV system with a varying time delay, which makes it difficult to control. The system can be discretized into a discrete-time LTV system with time delay by Zero-Order Holder (ZOH) method. Due to the assumption that the variations of speeds are relatively small in the R2R system described in Sec II, the upstream roller rotates by an approximately constant angle, i.e.

$$\delta\theta = \int_{\tau}^{\tau+\delta\tau} v_i(\tau) d\tau \approx v_i^r \delta\tau \quad (9)$$

where $\delta\tau$ is the discrete time step. When $\delta\tau$ is relatively small, we can transform the discrete-time system into an approximate discrete-angle system in the spatial domain in terms of $\delta\tau$.

By transforming the original system into a discrete system based on discretized angle step $\delta\tau$, the repetitiveness can be found in the spatial domain and it makes the control problem suitable for ILC methods. Consider in general the angle-varying linear discrete system

$$\begin{aligned} x_j(\theta + 1) &= A_j(\theta)x_j(\theta) + B_j(\theta)u_j(\theta) \\ y_j(\theta) &= C_{2,j}(\theta)x_j(\theta) + C_{1,j-1}(\theta)x_{j-1}(\theta) \end{aligned} \quad (10)$$

where $\theta = 0, 1, \dots, N$, and the subscript j indicates the system iteration number. The output y_j is decided by both the states in the current iteration j and the last iteration $j - 1$, which corresponds to the time-delay effect in Eq. (6). Thus, the time-delay effect can be converted to the iteration propagation in Eq. (10).

To simplify the problem, we can assume the system matrices A_j , B_j , $C_{2,j}$, and $C_{1,j-1}$ are all iteration-invariant when a properly-designed PID controller is applied to the system (6) to stabilize it. Thus, the stabilized system becomes

$$\begin{aligned} x_j(\theta + 1) &= A(\theta)x_j(\theta) + B(\theta)u_j(\theta) \\ y_j(\theta) &= C_2(\theta)x_j(\theta) + C_1(\theta)x_{j-1}(\theta) \end{aligned} \quad (11)$$

Remark 3: TILC methods often require the rigorous repetitiveness of the controlled processes with bounded initial state

shifts. In practice, a process can be reset before the operation starts to ensure identical initial states. However, it limits the applications of TILC methods to continuous processes that cannot be reset. In our work, we use PID to stabilize the system instead of artificial resetting. The repetitiveness requirement and the initial state shift constraint for TILC can be satisfied by the PID component. A TILC component is then added to the control input signal to create a PID-TILC hybrid controller.

The terminal output we want to minimize is the integral of y_j over a fixed angle interval $[0, 2\pi]$. When the discretization step N is relatively large, the integral Y_j can be approximated as the following summation:

$$\begin{aligned} Y_j &= \sum_{k=1}^N y_j(k) \delta\theta \\ &= \sum_{k=1}^N C_2(k) x_j(k) \delta\theta + \sum_{k=1}^N C_1(k) x_{j-1}(k) \delta\theta \end{aligned} \quad (12)$$

where $\delta\theta = 2\pi/N$. It is reasonable to assume that the Y_j is bounded because the states such as tension and speed variation should be bounded in real-world R2R systems stabilized by properly-tuned PID controllers.

Assume that there exists an equilibrium control input profile $u_{eq}(\theta)$ over $[0, 2\pi]$ such that $x_i(\theta) = 0$ for $\theta = 0, 1, \dots, N$. In practical applications, we can only know a nominal equilibrium control input u_{eq}^* that is a constant vector solved from Eq. (5). Therefore, the introduced axis mismatch disturbance results in an iteration-invariant disturbance profile $u_{dist}(\theta), \theta = 0, 1, \dots, N$ to the control input in each iteration, i.e.

$$u_{dist}(\theta) = u_{eq}^* - u_{eq}(\theta) \quad (13)$$

This iteration-invariant disturbance profile u_{dist} will cause a fixed terminal output Y_{dist} . When the desired terminal output is set as Y_d , the terminal output error $E_j = Y_j - Y_d$ will be a constant value. In the R2R registration error problem, we set $Y_d = 0$. Thus, the control goal can be described by the following equation:

$$\lim_{j \rightarrow \infty} Y_j = 0 \quad (14)$$

Remark 4: Theoretically, Y_{dist} can be adjusted by tuning the PID controller, but it requires manual tuning work case by case and it is often difficult to realize in practical applications. Also, the PID controller cannot track the change of Y_d when Y_d is not a fixed value through iterations.

To address the problem in Remark 4, we add an STILC component to the control input. The iterative updating law is the P-type ILC updating law with a pre-defined basis function:

$$u_{j+1}^{STILC}(\theta) = u_j^{STILC}(\theta) + \mathcal{L}\Phi(\theta)E_j \quad (15)$$

where $u_{j+1}^{STILC}(\theta)$ is the STILC control input component when the phase angle is θ for the $(j+1)^{th}$ iteration (current iteration), $u_j^{STILC}(\theta)$ is the STILC control input at the same phase angle for the j^{th} iteration (last iteration), \mathcal{L} is the learning gain, E_j is the terminal output error generated in

the j^{th} iteration (last iteration). In the R2R registration error problem, E_j is the registration error $r_{i,j}$ measured at the end of the j^{th} operation cycle. Φ is a properly-selected basis function matrix

$$\Phi(\theta) = \begin{bmatrix} \phi_1(\theta) \\ \phi_2(\theta) \\ \vdots \\ \phi_n(\theta) \end{bmatrix} \quad (16)$$

where n is the dimension of the input vector, $\phi_1(\theta), \phi_2(\theta), \dots, \phi_n(\theta)$ are $R \rightarrow R$ functions.

B. Stability Analysis

By solving Eq. (11), we obtain the transition equation from the initial state

$$x_j(k) = G(k)x_j(0) + H(k)\Xi_j + H_d(k) \quad (17)$$

where $G(k)$ and $H(k)$ can be obtained by the following recursive calculations:

$$\begin{aligned} G(k+1) &= A(k)G(k), G(0) = I, \\ H(k+1) &= A(k)H(k) + B(k)\Phi(k), H(0) = 0, \\ H_d(k+1) &= A(k)H_d(k) + B(k)u_{dist}(k), \\ H_d(0) &= B(0)u_{dist}(0), k = 0, 1, \dots, N-1 \end{aligned} \quad (18)$$

and Ξ_j can be obtained by the following iterative updating equation:

$$\Xi_j = \Xi_{j-1} + \mathcal{L}E_{j-1}, \Xi_0 = 0, j = 1, 2, \dots \quad (19)$$

Substituting (17) into (12), we get

$$\begin{aligned} Y_j &= \left[\sum_{k=1}^N C_2(k)G(k)x_j(0) + \sum_{k=1}^N C_1(k)G(k)x_{j-1}(0) \right] \delta\theta \\ &\quad + \sum_{k=1}^N [C_2(k) + C_1(k)]H_d(k) \delta\theta \\ &\quad + \left[\sum_{k=1}^N C_2(k)H(k) + \sum_{k=1}^N C_1(k)H(k) \right] \delta\theta \Xi_{j-1} \\ &\quad + \sum_{k=1}^N C_2(k)H(k) \delta\theta \mathcal{L}E_{j-1} \end{aligned} \quad (20)$$

If the desired terminal output Y_d is given, based on (17)(18)(19) we can get

$$\begin{aligned} E_j &= Y_j - Y_d \\ &= \Omega_1 E_{j-1} + \Omega_2 \sum_{s=1}^{j-2} E_s + \Omega_3 \end{aligned} \quad (21)$$

where

$$\begin{aligned}
\Omega_1 &= \sum_{k=1}^N C_2(k)H(k)\delta\theta\mathcal{L} \\
\Omega_2 &= \left[\sum_{k=1}^N C_2(k)H(k) + \sum_{k=1}^N C_1(k)H(k) \right] \delta\theta \\
\Omega_3 &= \left[\sum_{k=1}^N C_2(k)G(k)x_j(0) + \sum_{k=1}^N C_1(k)G(k)x_{j-1}(0) \right] \delta\theta + \\
&\quad \sum_{k=1}^N [C_2(k) + C_1(k)]H_d(k)\delta\theta - Y_d
\end{aligned} \tag{22}$$

In the following theorem, we show that E_j converges to zero when Ω_1 and Ω_2 satisfy a specific criterion. This theorem represents a pivotal finding in our research, as it establishes the fundamental conditions under which R2R systems can effectively reduce registration errors. This theorem applies to multi-layer manufacturing processes that are governed by the LTV system (11) and the second-order terminal output dynamics (12). Different from typical ILC problems where resetting operation is applied to restoring a constant initial state for each iteration, the continuously running R2R system cannot clean up the information generated in the last iteration by resetting at the end of the operation cycle. The information in the last iteration (e.g. the printed position or the deposition height of the last layer) is propagated to the current iteration and influences the terminal output for the current iteration. By applying STILC to these processes, we derive the convergence criterion by analyzing the convergence of a second-order recurrence series, as described in (26).

Theorem 1: Consider a stabilized discrete LTV system (11) and a given achievable terminal output Y_d integrated as (12). Through the repetitive operation cycles, the STILC law in (15) will make the terminal error E_j converge to zero if $|\lambda_1| < 1$ and $|\lambda_2| < 1$, where λ_1, λ_2 are the two roots of the following characteristic equation

$$\lambda^2 - (\Omega_1 + 1)\lambda + (\Omega_1 - \Omega_2) = 0. \tag{23}$$

Proof: By (21) we can derive

$$E_{j+1} = \Omega_1 E_j + \Omega_2 \sum_{s=1}^{j-1} E_s + \Omega_3. \tag{24}$$

Since the system (11) is stabilized, we can assume the initial state $x_j(0)$ for any iteration j is identical. Subtracting (21) from (24) yields

$$E_{j+1} - E_j = \Omega_1 E_j - \Omega_1 E_{j-1} + \Omega_2 E_{j-1}. \tag{25}$$

Rearranging (32), we obtain

$$E_{j+1} - (\Omega_1 + 1)E_j + (\Omega_1 - \Omega_2)E_{j-1} = 0. \tag{26}$$

Thus, the terminal error satisfies a second-order recurrence relation. We can obtain the general solution [43] for the second-order recurrence relation (26).

If $\lambda_1 \neq \lambda_2$, then the general solution is

$$E_j = \xi_1 \lambda_1^j + \xi_2 \lambda_2^j. \tag{27}$$

If $\lambda_1 = \lambda_2 = \lambda_0$, then the general solution is

$$E_j = (\xi_1 + \xi_2 j) \lambda_0^j. \tag{28}$$

ξ_1 and ξ_2 are two bounded complex numbers and can be solved when the first two errors E_0, E_1 are known.

From the general solutions (27) and (28), it is obvious that $\lim_{j \rightarrow \infty} E_j = 0$ if $|\lambda_1| < 1$ and $|\lambda_2| < 1$. ■

Remark 5: From Theorem 1, we know the convergence performance of the terminal error E_j is decided by two parameters, Ω_1 and Ω_2 . When designing the controller, we can design different basis function matrices Φ and learning gains \mathcal{L} to tune Ω_1 and Ω_2 . Based on Theorem 1, we can derive some specific rules to help us design the appropriate basis function matrix and learning gain.

C. Basis Function Design and Learning Gain Selection

Ideally, we expect the designed STILC to fully compensate u_{dist} once it detects any terminal error so that any fluctuations in tensions or speeds can be fully eliminated, as well as the registration error. As we define $\Xi_0 = 0$ in (19), the STILC will not generate any compensation signal in the first iteration. At the end of the first iteration, it detects the terminal error and starts to generate a compensation signal for the second iteration. Thus, the ideal Φ and \mathcal{L} should satisfy the following relation:

$$\Phi(k)\mathcal{L}E_1 = -u_{dist}(k), k = 0, 1, \dots, N-1. \tag{29}$$

Thereafter, any fluctuations or the terminal error can be eliminated after just one iteration. However, it is difficult to obtain an exact u_{dist} profile in practical applications. In the following, we state that it is acceptable if an approximate basis function matrix can be designed based on some prior knowledge or observations about the process. For example, in a rotary system with axis mismatches, we can use trigonometric functions as the basis functions.

The transition equation (17) can be rewritten to include u_j and u_{dist} explicitly:

$$x_j(k) = G(k)x_j(0) + \mathcal{H}(k)[\tilde{u}_j(k) + \tilde{u}_{dist}] \tag{30}$$

where $\tilde{u}_j(k) = [u_j(0) \ u_j(1) \ u_j(2) \ \dots \ u_j(k-1) \ 0 \ \dots]^T$ is a truncated profile of control input u . \tilde{u}_{dist} is similar. And we know

$$\tilde{u}_j(k) = \tilde{u}_0(k) + \Xi_j \tilde{\Phi}(k) \tag{31}$$

where $\tilde{\Phi}(k) = [\Phi(0) \ \Phi(1) \ \Phi(2) \ \dots \ \Phi(k-1) \ 0 \ \dots]^T$.

We can also write $\tilde{u}_j(k)$, \tilde{u}_{dist} , and $\tilde{\Phi}(k)$ as the multiplication of a matrix M_k and the complete profiles:

$$\begin{aligned}
\tilde{u}_j(k) &= M_k u_j \\
\tilde{u}_{dist} &= M_k u_{dist} \\
\tilde{\Phi}(k) &= M_k \Phi
\end{aligned} \tag{32}$$

where M_k is

$$M_k = \begin{bmatrix} I_k & \mathbf{0} \\ \mathbf{0} & \mathbf{0} \end{bmatrix}_{N \times N} \tag{33}$$

Rearranging (20), we can obtain

$$\begin{aligned}
Y_j / \delta\theta &= \sum_{k=1}^N [C_2(k)G(k)x_j(0) + C_1(k)G(k)x_{j-1}(0)] \\
&+ \sum_{k=1}^N [C_2(k)\mathcal{H}(k)M_k]\Delta u_{j-1} \\
&+ \sum_{k=1}^N [C_2(k)\mathcal{H}(k)M_k + C_2(k)\mathcal{H}(k)M_k](\Xi_{j-1}\Phi + u_{dist})
\end{aligned} \tag{34}$$

Note that X_i is a scalar and Φ is a $N \times 1$ vector in this work. The STILC updating law aims to approach a Ξ iteratively making Y converge to the desired value (zero in this problem). Let $\mathcal{N} = \sum_{k=1}^N [C_2(k)\mathcal{H}(k)M_k + C_2(k)\mathcal{H}(k)M_k]$. We can confirm the existence of such a Ξ as stated in the following theorem:

Theorem 2: If the designed basis function vector Φ satisfies $\mathcal{N}\Phi \neq 0$, then there exists a Ξ such that $Y = 0$.

In this problem, we can further assume that the initial states of iterations, $x_{j-1}(0)$ and $x_j(0)$, are zero. When convergence has been achieved, the second term in (34) is also zero because $\Delta u_{j-1} = 0$. If Φ and u_{dist} are parallel vectors, it is evident that there exists a solution Ξ making $(\Xi\Phi + u_{dist})$ zero. If there is a small angle between Φ and u_{dist} , we should still be able to find a solution Ξ making $(\Xi\Phi + u_{dist})$ orthogonal to \mathcal{N} . The process of convergence in the iteration domain becomes solving a linear equation with one unknown variable, which is considered easy to solve numerically. This is the fundamental reason for the simplicity of the proposed STILC design.

Compared with designing an ideal basis function vector Φ in (29) that generates a completely opposite signal to u_{dist} , it is easier for practitioners to tune the learning gain \mathcal{L} to make Ω_1 and Ω_2 satisfy the criteria of convergence in Theorem 1.

Solving (23), we can get the two characteristic roots:

$$\begin{aligned}
\lambda_1 &= \frac{1}{2}[\Omega_1 + 1 + \sqrt{(\Omega_1 - 1)^2 + 4\Omega_2}] \\
\lambda_2 &= \frac{1}{2}[\Omega_1 + 1 - \sqrt{(\Omega_1 - 1)^2 + 4\Omega_2}]
\end{aligned} \tag{35}$$

For the two roots, there are the following two cases.

Case 1: $(\Omega_1 - 1)^2 + 4\Omega_2 \geq 0$

TABLE I: Simulation Parameters

Parameter	Notation	Value
Cross-sectional Area	A	$1.29 \times 10^{-5} \text{ m}^2$
Young's Modulus	E	186.158 MPa
Reference Roller Radius	R_i^r, R_{i+1}	0.381 m
Inertia of Roller	J_i, J_{i+1}	0.146 kg·m ²
Friction Coefficient	f_i, f_{i+1}	0.685
Gear Ratio	n_i, n_{i+1}	1
Span Length	L_i, L_{i+1}, L_{i+2}	2.4 m
Reference Speed	v_i^r, v_{i+1}^r	0.16 m/s
Reference Tension	$t_i^r, t_{i+1}^r, t_{i+2}^r$	20 N
Reference Period Time	τ_i^r	14.962 s

In this case, λ_1 and λ_2 are real numbers. In order to satisfy $|\lambda_1| < 1$ and $|\lambda_2| < 1$, we need

$$\begin{aligned}
\frac{1}{2}[\Omega_1 + 1 + \sqrt{(\Omega_1 - 1)^2 + 4\Omega_2}] &< 1 \\
\frac{1}{2}[\Omega_1 + 1 - \sqrt{(\Omega_1 - 1)^2 + 4\Omega_2}] &> 1.
\end{aligned} \tag{36}$$

From (36) and the condition for Case 1, we obtain $-3 < \Omega_1 < 1$ and $\Omega_2 < 0$.

Case 2: $(\Omega_1 - 1)^2 + 4\Omega_2 < 0$

In this case, λ_1 and λ_2 are complex numbers. In order to satisfy $|\lambda_1| < 1$ and $|\lambda_2| < 1$, we need

$$\frac{1}{4}(\Omega_1 + 1)^2 - \frac{1}{4}[(\Omega_1 - 1)^2 + 4\Omega_2] < 1 \tag{37}$$

From (37) and the condition for Case 2, we obtain $\Omega_1 < 1$ and $\Omega_2 < 0$.

It is evident that $\Omega_2 < 0$ is required in both cases. Therefore, once an approximate basis function matrix Φ is defined, the first critical step in designing the learning gain \mathcal{L} is to determine the correct sign for \mathcal{L} . An incorrect sign will prevent any possibility of achieving convergence. Then we can increase the absolute value of \mathcal{L} as much as possible, as a higher learning gain enhances the responsiveness of STILC and increases the learning speed. However, setting the learning gain too high can lead to significant overshoot or even result in divergence. To prevent these issues, we set the learning gain to satisfy $(\Omega_1 - 1)^2 + 4\Omega_2 = 0$. In section IV, we show the effects of different learning gain selections.

IV. SIMULATION VERIFICATION

To thoroughly verify and validate the proposed STILC-PID method, We develop a numerical model of a two-roller R2R printing system in Simulink and configure the parameters as shown in Table I. The simulation results are then discussed.

A. Non-Zero RE Convergence Performance from Feedback Control Methods

In [14], a decentralized controller is designed to regulate the speeds and tensions in the R2R system. Figure 6 shows the schematic of the decentralized control scheme for a two-roller system. The control input signal for each roller motor is the summation of two components: (a) the open-loop component

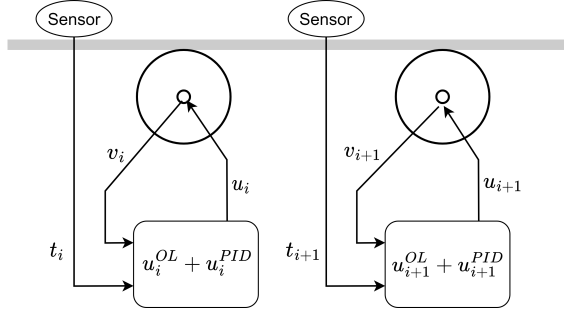


Fig. 6: Decentralized PID Control for Tension and Speed Regulation

given by Eq. (4), and (b) the closed-loop component generated by a PID controller.

The control law of the decentralized controller for gravure printing roller i and roller $(i + 1)$ is given as the following:

$$\begin{aligned}
 u_i(\tau) &= u_i^{OL} + u_i^{PID}(\tau) \\
 u_i^{OL} &= u_i^r \\
 u_i^{PID}(\tau) &= K_i^P [T_i(\tau) \quad V_i(\tau)]^T \\
 &\quad + K_i^I \left[\int_0^\tau T_i(\tau) d\tau \quad \int_0^\tau V_i(\tau) d\tau \right]^T \\
 &\quad + K_i^D [\dot{T}_i(\tau) \quad \dot{V}_i(\tau)]^T \\
 u_{i+1}(\tau) &= u_{i+1}^{OL} + u_{i+1}^{PID}(\tau) \\
 u_{i+1}^{OL} &= u_{i+1}^r \\
 u_{i+1}^{PID}(\tau) &= K_{i+1}^P [T_{i+1}(\tau) \quad V_{i+1}(\tau)]^T \\
 &\quad + K_{i+1}^I \left[\int_0^\tau T_{i+1}(\tau) d\tau \quad \int_0^\tau V_{i+1}(\tau) d\tau \right]^T \\
 &\quad + K_{i+1}^D [\dot{T}_{i+1}(\tau) \quad \dot{V}_{i+1}(\tau)]^T
 \end{aligned} \tag{38}$$

where u_i^{OL} and u_{i+1}^{OL} are the open-loop input components, u_i^{PID} and u_{i+1}^{PID} are the closed-loop input components provided by the decentralized PID, and K_i and K_{i+1} are the feedback gain vectors.

Figure 7 illustrates the temporal fluctuations of the five state variables described by Eq. (5) when an axis mismatch is introduced to the upstream roller. It should be noted that T_{i+1} and T_{i+2} overlap in this case. On the other hand, Figure 8 displays the registration error resulting from speed and tension fluctuations. It is important to emphasize that $r_i(\tau)$ represents a continuous function of time; however, it can only be measured by the sensor after the printing of the downstream pattern on the web. Consequently, the actual registration error is updated whenever the terminal condition is met, specifically when the phase angle of the gravure pattern on the downstream roller reaches 2π . Throughout the intermediate process of each iteration, the registration error remains constant after the initial update at the beginning of the iteration. As depicted in Figure 8b, the registration error accumulates and dilates iteratively when only the open-loop input component is applied to the system.

Then we compare the effects of decentralized PID controllers with different parameter settings. Given the similar dynamics of the upstream and downstream rollers, the two

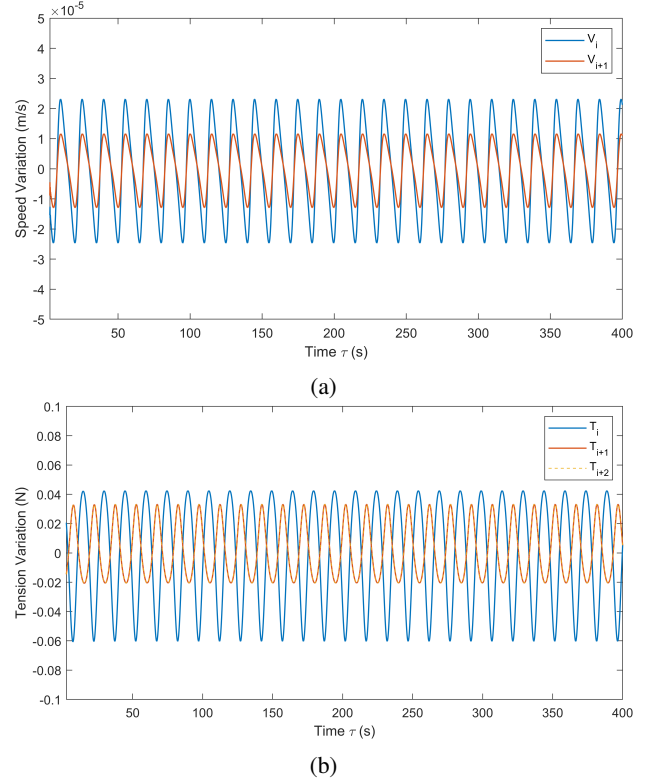


Fig. 7: Speed and Tension Variations Caused by Axis Mismatch. (a)Speed Variations; (b)Tension Variations

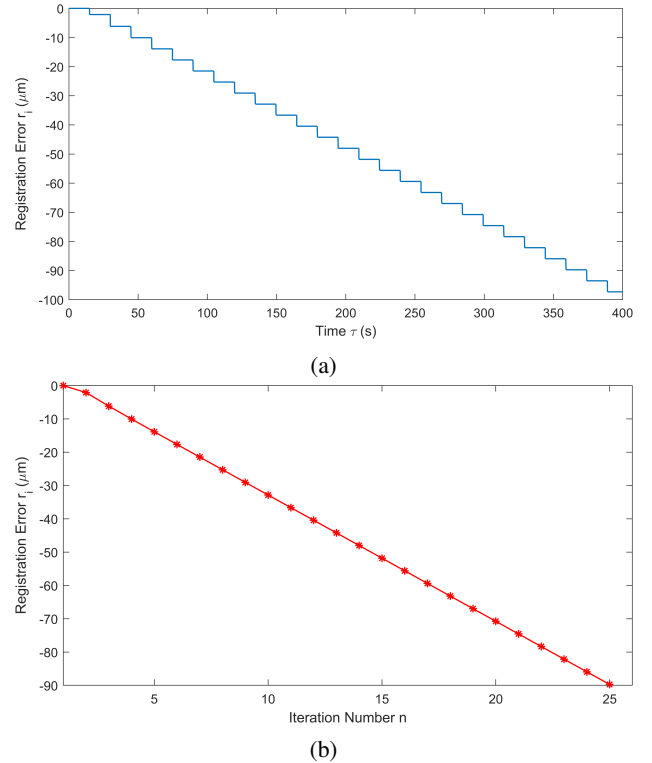


Fig. 8: Registration Error Caused by Axis Mismatch with Only Open-loop Control Input. (a) The actual registration error value in time domain; (b) Registration error in the iteration domain

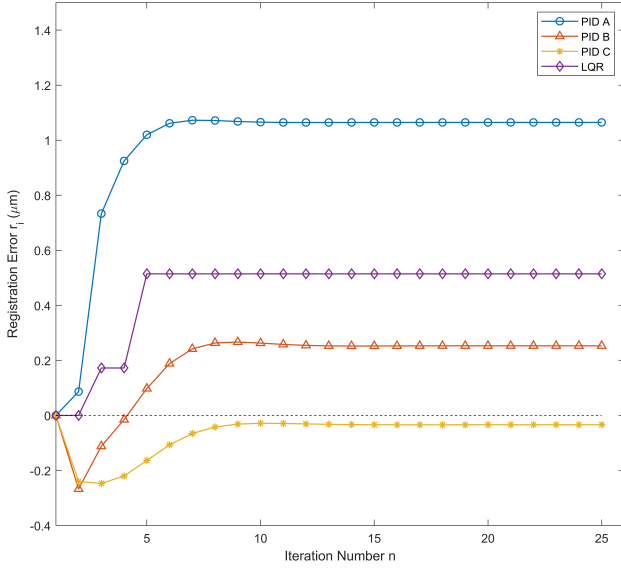


Fig. 9: Registration Error Controlled by Decentralized PID Controllers with Different Parameter Settings

TABLE II: Controller Settings

Setting	K^P	K^I	K^D
PID A	$[-0.1916 \ 0]$	$[-0.0767 \ 0]$	$[-0.0038 \ -0.1916]$
PID B	$[-0.1916 \ 0]$	$[-0.0575 \ 0]$	$[-0.0038 \ -0.1916]$
PID C	$[-0.3832 \ 0]$	$[-0.0575 \ 0]$	$[-0.0038 \ -0.1916]$

PID modules for the two rollers share the same parameter setting. In Figure 9, we compare the performances of three decentralized PID controllers with different parameter settings. The parameters are listed in Table II. Controller PID A exhibits the highest convergence error, demonstrating the least effective performance. In contrast, PID B and PID C show significantly improved performance, with PID C achieving a particularly low registration error level. Nonetheless, it should be noted that while the registration errors converge to constant values, convergence to zero is not assured. This observation aligns with the analysis presented in Remark 4. In engineering practice, it can be challenging for practitioners to find an optimal set of PID parameters that will precisely converge the registration error to zero. Additionally, the optimal PID parameters may need to be adjusted every time the system parameters changes.

Besides PID control, LQR is also a popular class of feedback control strategy to minimize a quadratic-form operation cost. The optimal control law can be derived from solving the Riccati Equation. We design an LQR controller by leveraging the continuous-time nominal model of the R2R system. Because the RE is related to the integral of tensions (see (6)), we augment the system with integral states:

$$\begin{bmatrix} \dot{x}(t) \\ \dot{z}(t) \end{bmatrix} = \begin{bmatrix} A_{nominal} & 0 \\ -C_{nominal} & 0 \end{bmatrix} \begin{bmatrix} x(t) \\ z(t) \end{bmatrix} + \begin{bmatrix} B_{nominal} \\ 0 \end{bmatrix} u(t) \quad (39)$$

where $z(t)$ represents the integral of the states. The matrices of the nominal system are:

$$A_{nominal} = \begin{bmatrix} -\frac{vr_1}{L_1} & 0 & 0 & \frac{AE-tr_1}{L_1} & 0 \\ \frac{vr_1}{L_2} & -\frac{vr_2}{L_2} & 0 & \frac{tr_1-AE}{L_2} & \frac{AE-tr_2}{L_2} \\ 0 & \frac{vr_2}{L_3} & -\frac{vr_3}{L_3} & 0 & \frac{tr_2-AE}{L_3} \\ -\frac{R_1^2}{J_1} & \frac{R_1^3}{J_1} & 0 & -\frac{bf_1}{J_1} & 0 \\ 0 & -\frac{R_2^2}{J_2} & \frac{R_2^3}{J_2} & 0 & -\frac{bf_2}{J_2} \end{bmatrix}$$

$$B_{nominal} = \begin{bmatrix} 0 & 0 \\ 0 & 0 \\ 0 & 0 \\ \frac{n_1 R_1}{J_1} & 0 \\ 0 & \frac{n_2 R_2}{J_2} \end{bmatrix}$$

$$C_{nominal} = \begin{bmatrix} 1 & 0 & 0 & 0 & 0 \\ 0 & 1 & 0 & 0 & 0 \end{bmatrix}$$

For the LQR design, we need the augmented system matrices

$$A_{aug} = \begin{bmatrix} A_{nominal} & 0 \\ -C & 0 \end{bmatrix}, \quad B_{aug} = \begin{bmatrix} B_{nominal} \\ 0 \end{bmatrix}$$

and we design the cost function:

$$J = \int_0^{\infty} (x_{aug}^T Q x_{aug} + u^T R u) dt \quad (40)$$

where $x_{aug} = [x \ z]^T$, and Q and R are positive definite weighting matrices. In the following simulation, we define Q and R as

$$Q = \begin{bmatrix} 10 & 0 & 0 & 0 & 0 & 0 & 0 \\ 0 & 10 & 0 & 0 & 0 & 0 & 0 \\ 0 & 0 & 1 & 0 & 0 & 0 & 0 \\ 0 & 0 & 0 & 1 & 0 & 0 & 0 \\ 0 & 0 & 0 & 0 & 1 & 0 & 0 \\ 0 & 0 & 0 & 0 & 0 & 100 & 0 \\ 0 & 0 & 0 & 0 & 0 & 0 & 100 \end{bmatrix}$$

$$R = \begin{bmatrix} 5 & 0 \\ 0 & 5 \end{bmatrix}$$

Then we solve the algebraic Riccati equation:

$$A_{aug}^T P + P A_{aug} - P B_{aug} R^{-1} B_{aug}^T P + Q = 0 \quad (41)$$

The positive definite matrix P solved from (41) can be used to calculate the optimal feedback gain $K_{LQR} = R^{-1} B_{aug}^T P$. The final control law is given by:

$$u(t) = -K_{LQR} \begin{bmatrix} x(t) \\ z(t) \end{bmatrix} \quad (42)$$

The purple line in Figure 9 shows the performance of the LQR controller designed above. As observed with the PID controllers, the LQR controller similarly results in RE convergence to a non-zero steady-state value. Despite augmenting the state vector with integral terms in the LQR design, the controller remains insufficient to fully capture the complex RE dynamics and achieve complete elimination. This motivates us to add an additional STILC component to further improve the RE mitigation performance.

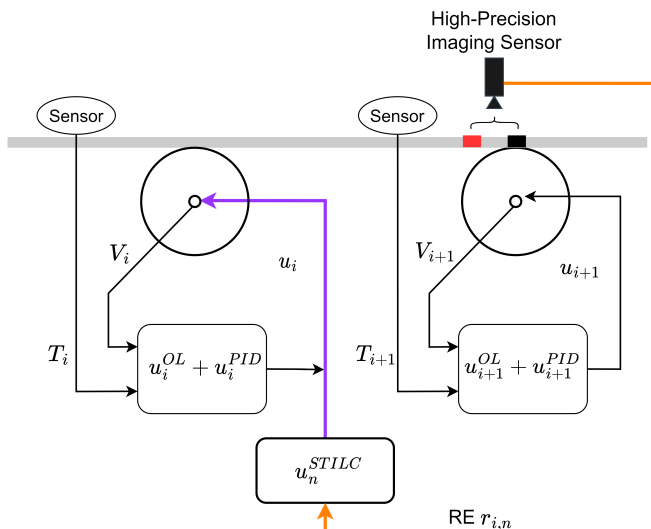


Fig. 10: STILC-PID Hybrid Control for Registration Error

B. Successful RE Elimination by Adding STILC Components

To guarantee that the registration converges to zero, we add a STILC component to the control input of the upstream roller, as shown in Figure 10. As the target of this work is to propose a simplest pipeline of designing effective controllers to eliminate RE, we select PID as the baseline controller which requires much less expert knowledge than designing a LQR controller. Figure 11 shows the comparison between the registration control performances between the STILC-PID hybrid controller and the pure decentralized PID controllers with different PID parameter settings. The specific controller settings are given in Table III. The simulation results show that the proposed hybrid controller with an additional STILC input component makes the registration error converge to zero after sufficient iterations (10-20 iterations in this simulation case). For PID A, the worst PID parameter setting in these three settings, an additional STILC component significantly reduces the registration error in 10 iterations and makes the error converge to zero, as shown in Figure 11a. Similar effects can be observed for PID B and PID C settings in Figure 11b and Figure 11c. For PID C, even though the purely decentralized PID achieves a relatively small registration error, the STILC-PID hybrid controller enhances the accuracy further. It completely eliminates the registration error after undergoing several oscillations in the iteration domain. It is worth noting that the added STILC is also effective for LQR controller, as observed in Figure 11d, which implies the generalizability of the STILC component. Therefore, the proposed hybrid controller shows a significant advantage in R2R printing registration control.

The control law of the hybrid controller is given as follows:

$$u_j(\tau) = u_j^{OL} + u_j^{PID}(\tau) + u_n^{STILC}(\theta_i(\tau)) \quad (43)$$

C. Comparison of the Effects of Different Learning Gains

To make the STILC more feasible in real-world scenarios, we design a discretized basis function as shown in Fig. 12.

TABLE III: PID and STILC Settings

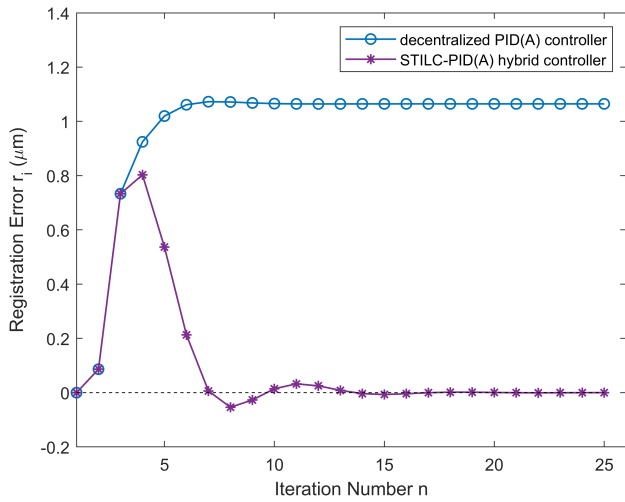
Setting	Notation	Value
PID Gain (P)	K_i^P, K_{i+1}^P	$[-0.1916 \quad 0]$
PID Gain (I)	K_i^I, K_{i+1}^I	$[-0.0767 \quad 0]$
PID Gain (D)	K_i^D, K_{i+1}^D	$[-0.0038 \quad -0.1916]$
ILC Learning Gain	P	5000
Basis Function	G	Shown in Fig. 12 (20-step)

The discretized basis function can be written in the memory of the controller hardware as a small lookup table. Thus, it can help avoid computing the cosine function in real-time. Figure 11 demonstrates that a 20-step discretized cosine-form basis function adequately approximates the disturbance profile u_{dist} , enabling the registration error to iteratively converge to zero, as we discuss in Eq. (29). We also discuss the influence of learning gain selection in Section III. Figure 13 compares the effects of selecting different learning gains. It shows that a negative learning gain (-100) will make the registration error diverge, while positive learning gains (3000, 5000, 7000) can make the registration error converge to zero. Larger learning gains give us a faster response in the iteration domain and reduce the registration error more aggressively, but also cause larger overshoot and fluctuations. By numerical computation, we know selecting $\mathcal{L} = 5000$ approximately satisfies $(\Omega_1 - 1)^2 + 4\Omega_2 = 0$. And the simulation result shows $\mathcal{L} = 5000$ can provide balanced performance for convergence speed and fluctuation. A smaller learning gain can be selected if a monotonic and asymptotic convergence is required, such as $\mathcal{L} = 3000$. These results have verified our analysis of the learning gain selection principle at the end of Section III.

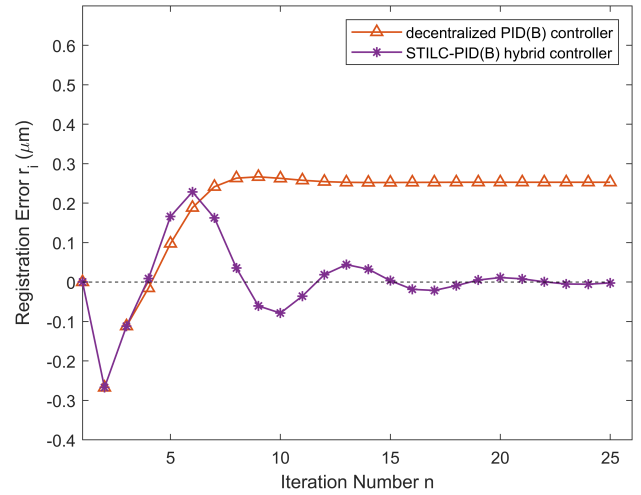
V. CONCLUSION

This paper presents a novel Spatial-Terminal Iterative Learning Control (STILC)-PID hybrid control method to address a fundamental challenge in registration control within Roll-to-Roll (R2R) printing systems: the inability to monitor real-time registration error (RE). The proposed method overcomes this limitation by incorporating a Terminal Iterative Learning Control (TILC) updating law with a spatially dependent basis function, enabling iterative convergence of the RE to zero. This approach contrasts with PID type of feedback control methods, which can only achieve convergence to a non-zero level.

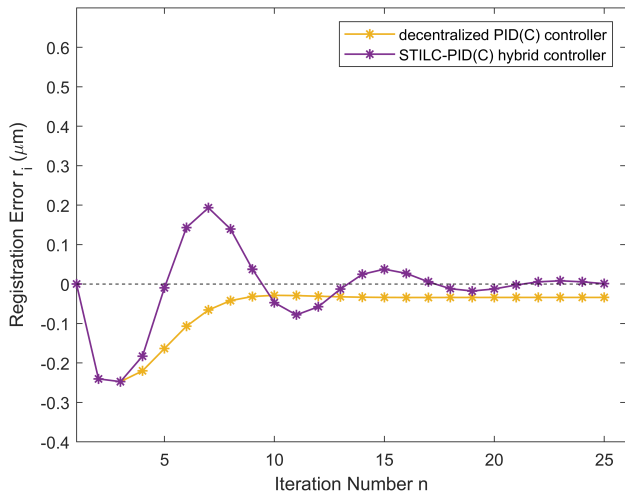
Our work builds upon the concept of Spatial Iterative Learning Control (SILC), adapting it specifically for R2R printing processes. We leverage the insight that rollers in R2R systems exhibit spatially (angularly) periodic behavior, a characteristic common to rotary machinery. This allows us to design a cosine-form basis function in the spatial domain, forming the foundation of our STILC method. The paper derives controller design criteria to ensure the convergence of the proposed STILC-PID hybrid control approach. These criteria provide clear guidance for practitioners to design the basis function and select the proper learning gain, significantly simplifying the controller design process. This feature is particularly beneficial for broadening the applicability of STILC to various repetitive manufacturing processes governed by linear time-varying (LTV) dynamics.



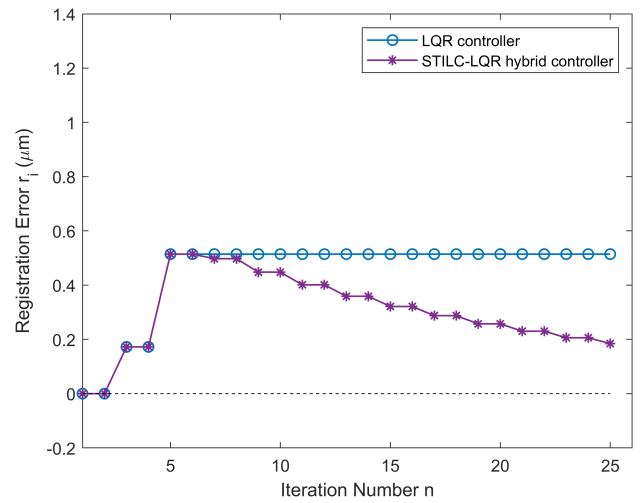
(a)



(b)



(c)



(d)

Fig. 11: Performance Comparison between Proposed STILC-based Hybrid Controller and the pure feedback controllers Controllers (a) PID A; (b) PID B; (c) PID C; (d) LQR

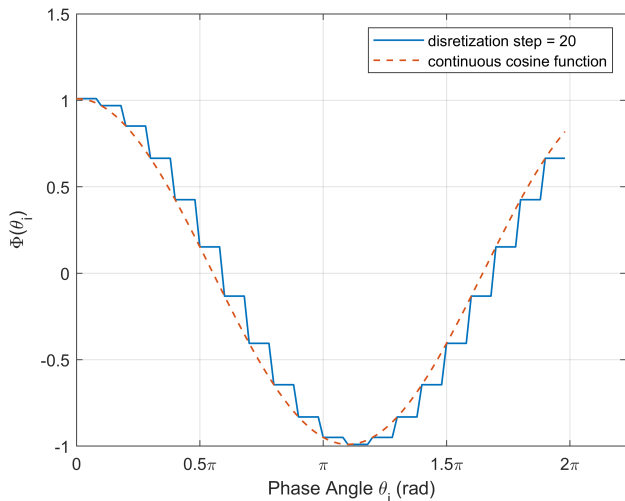


Fig. 12: 20-Step Discretized Cosine-Form Basis Function

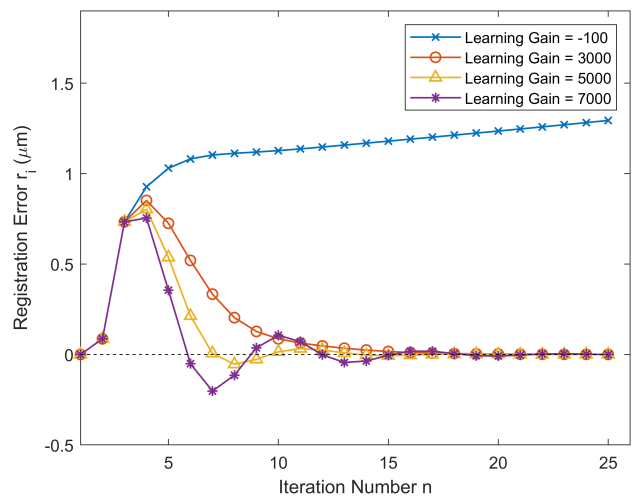


Fig. 13: Learning Gain Effects Comparison

To evaluate the effectiveness of our method, we apply it to a registration control problem in R2R printing systems. We employ the perturbation method to model the dynamics of the RE and the R2R system. Additionally, we introduce a common source of disturbance—a spatially-dependent axis mismatch between the motor shaft and the roller center. Through simulation experiments conducted in Simulink, we demonstrate the effectiveness of the proposed STILC-PID hybrid control method. The simulation results clearly show that our method achieves convergence of the RE to zero in the iteration domain, while the traditional decentralized PID method only achieves convergence to a non-zero value. Our STILC method offers several key advantages over existing approaches:

(1) It is a learning-based data-driven control method, minimizing requirements on designers' expertise and hardware computation capabilities.

(2) It updates the control input profile by adjusting only one parameter based on the terminal RE measurement, significantly reducing the computational burden for real-time control.

(3) It provides a highly simplified approach to controller design, enhancing its accessibility to practitioners across various applications while maintaining its effectiveness.

As part of future work, we plan to enhance our method to handle practical disturbances encountered in R2R printing systems, such as roller roundness errors and axis mismatches with varying initial phase angles. Moreover, we intend to validate the proposed method in industrial application scenarios involving general rotary machine systems, which inherently exhibit angle-periodic behaviors.

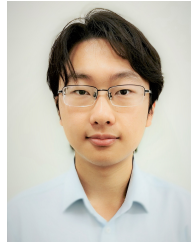
Our proposed STILC method holds significant promise as a solution to widespread industrial problems since angle-periodic behaviors broadly exist in various machines driven by motors. For example, in multi-axis motion systems, such as those used in Computer Numerical Control (CNC) machining, advanced robotics, and 3D printing, the tool paths or actuator trajectories are essentially determined by the angle-periodic behaviors of drive motors. Our method presents a suitable solution to compensate for angle-dependent repetitive disturbances and help achieve better precision across these diverse applications.

REFERENCES

- [1] C.-M. Chen, S. Anastasova, K. Zhang, B. G. Rosa, B. P. L. Lo, H. E. Assender, and G.-Z. Yang, "Towards wearable and flexible sensors and circuits integration for stress monitoring," *IEEE Journal of Biomedical and Health Informatics*, vol. 24, no. 8, pp. 2208–2215, 2020.
- [2] S. Kwon, D. Song, H. Kim, M. Lee, and K. Woo, "Development of roll-to-roll multi-layer thermal evaporation system for flexible oled devices," in *2018 25th International Workshop on Active-Matrix Flatpanel Displays and Devices (AM-FPD)*, 2018, pp. 1–2.
- [3] D. L. Wood III, M. Wood, J. Li, Z. Du, R. E. Ruther, K. A. Hays, N. Muralidharan, L. Geng, C. Mao, and I. Belharouak, "Perspectives on the relationship between materials chemistry and roll-to-roll electrode manufacturing for high-energy lithium-ion batteries," *Energy Storage Materials*, vol. 29, pp. 254–265, 2020.
- [4] F. D. Giacomo, H. Fledderus, H. Gorter, G. Kirchner, I. d. Vries, I. Dogan, W. Verhees, V. Zardetto, M. Najafi, D. Zhang, H. Lifka, Y. Galagan, T. Aernouts, S. Veenstra, P. Groen, and R. Andriess, "Large area \dot{c} 140 cm² perovskite solar modules made by sheet to sheet and roll to roll fabrication with 14.5
- [5] M. Salari and M. Joodaki, "Investigation of electrical characteristics dependency of roll-to-roll printed solar cells with silver electrodes on mechanical tensile strain," *IEEE Transactions on Device and Materials Reliability*, vol. 19, no. 4, pp. 718–722, 2019.
- [6] M. Yang, H. Li, J. Wang, W. Shi, Q. Zhang, H. Xing, W. Ren, B. Sun, M. Guo, E. Xu *et al.*, "Roll-to-roll fabricated polymer composites filled with subnanosheets exhibiting high energy density and cyclic stability at 200° c," *Nature Energy*, vol. 9, no. 2, pp. 143–153, 2024.
- [7] E. Parvazian and T. Watson, "The roll-to-roll revolution to tackle the industrial leap for perovskite solar cells," *nature communications*, vol. 15, no. 1, p. 3983, 2024.
- [8] M. K. Välimäki, E. Jansson, V. J. Von Morgen, M. Ylikunnari, K.-L. Väisänen, P. Ontero, M. Kehusmaa, P. Korhonen, and T. M. Kraft, "Accuracy control for roll and sheet processed printed electronics on flexible plastic substrates," *The International Journal of Advanced Manufacturing Technology*, vol. 119, no. 9, pp. 6255–6273, 2022.
- [9] Z. Chen, T. Zhang, Y. Zheng, D. S.-H. Wong, and Z. Deng, "Fully decoupled control of the machine directional register in roll-to-roll printing system," *IEEE Transactions on Industrial Electronics*, vol. 68, no. 10, pp. 10 007–10 018, 2021.
- [10] Z. Chen, Y. Zheng, T. Zhang, D. S.-H. Wong, and Z. Deng, "Modeling and register control of the speed-up phase in roll-to-roll printing systems," *IEEE Transactions on Automation Science and Engineering*, vol. 16, no. 3, pp. 1438–1449, 2018.
- [11] H. Kang, C. Lee, and K. Shin, "Modeling and compensation of the machine directional register in roll-to-roll printing," *Control Engineering Practice*, vol. 21, no. 5, pp. 645–654, 2013.
- [12] Z. Chen, B. Qu, B. Jiang, S. R. Forrest, and J. Ni, "Robust constrained tension control for high-precision roll-to-roll processes," *ISA Transactions*, vol. 136, pp. 651–662, 2023. [Online]. Available: <https://www.sciencedirect.com/science/article/pii/S0019057822006127>
- [13] K. Shah, A. He, Z. Wang, X. Du, and X. Jin, "Data-driven model predictive control for roll-to-roll process register error," in *International Manufacturing Science and Engineering Conference*, vol. 86601. American Society of Mechanical Engineers, 2022, p. V001T03A006.
- [14] P. R. Pagilla, N. B. Siraskar, and R. V. Dvivedula, "Decentralized control of web processing lines," *IEEE Transactions on control systems technology*, vol. 15, no. 1, pp. 106–117, 2006.
- [15] M. Zhou, Z. Chen, Y. Zheng, and L. Zou, "Model based pd control during the speed-up phase in roll-to-roll web register systems," in *Proceedings of the 33rd Chinese Control Conference*, 2014, pp. 5139–5143.
- [16] D. A. Bristow, M. Tharayil, and A. G. Alleyne, "A survey of iterative learning control," *IEEE control systems magazine*, vol. 26, no. 3, pp. 96–114, 2006.
- [17] E. Sutanto and A. G. Alleyne, "Norm optimal iterative learning control for a roll to roll nano/micro-manufacturing system," in *2013 American Control Conference*. IEEE, 2013, pp. 5935–5941.
- [18] —, "Vision based iterative learning control for a roll to roll micro/nano-manufacturing system," *IFAC Proceedings Volumes*, vol. 47, no. 3, pp. 7202–7207, 2014.
- [19] C. Kim, S. W. Jeon, and C. H. Kim, "Measurement of position accuracy of engraving in plate roller and its effect on register accuracy in roll-to-roll multi-layer printing," *Measurement Science and Technology*, vol. 28, no. 12, p. 125002, 2017.
- [20] J. Lee, J. Seong, J. Park, S. Park, D. Lee, and K.-H. Shin, "Register control algorithm for high resolution multilayer printing in the roll-to-roll process," *Mechanical Systems and Signal Processing*, vol. 60, pp. 706–714, 2015.
- [21] J. Lee, S. Park, K.-H. Shin, and H. Jung, "Smearing defects: a root cause of register measurement error in roll-to-roll additive manufacturing system," *The International Journal of Advanced Manufacturing Technology*, vol. 98, no. 9, pp. 3155–3165, 2018.
- [22] S. Arimoto, S. Kawamura, and F. Miyazaki, "Bettering operation of robots by learning," *Journal of Robotic systems*, vol. 1, no. 2, pp. 123–140, 1984.
- [23] —, "Bettering operation of dynamic systems by learning: A new control theory for servomechanism or mechatronics systems," in *The 23rd IEEE Conference on Decision and Control*, 1984, pp. 1064–1069.
- [24] J. Han, D. Shen, and C.-J. Chien, "Terminal iterative learning control for discrete-time nonlinear systems based on neural networks," *Journal of the Franklin Institute*, vol. 355, no. 8, pp. 3641–3658, 2018.
- [25] J.-X. Xu, Y. Chen, T. H. Lee, and S. Yamamoto, "Terminal iterative learning control with an application to rtpcvd thickness control," *Automatica*, vol. 35, no. 9, pp. 1535–1542, 1999.

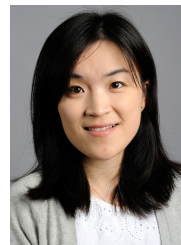
- [26] J. Han, D. Shen, and C.-J. Chien, "Terminal iterative learning control for discrete-time nonlinear system based on neural networks," in *2015 34th Chinese Control Conference (CCC)*, 2015, pp. 3190–3195.
- [27] X. Bu, J. Liang, Z. Hou, and R. Chi, "Data-driven terminal iterative learning consensus for nonlinear multiagent systems with output saturation," *IEEE Transactions on Neural Networks and Learning Systems*, vol. 32, no. 5, pp. 1963–1973, 2021.
- [28] R. Chi, D. Wang, Z. Hou, and S. Jin, "Data-driven optimal terminal iterative learning control," *Journal of Process Control*, vol. 22, no. 10, pp. 2026–2037, 2012.
- [29] Z. Wang and X. Jin, "Spatial-terminal iterative learning control for registration error elimination in high-precision roll-to-roll printing systems," in *International Manufacturing Science and Engineering Conference*, vol. 87240. American Society of Mechanical Engineers, 2023, p. V002T05A009.
- [30] J.-X. Xu and D. Huang, "Spatial periodic adaptive control for rotary machine systems," *IEEE Transactions on Automatic Control*, vol. 53, no. 10, pp. 2402–2408, 2008.
- [31] Z. Afkhami, C. Pannier, L. Aarnoudse, D. Hoelzle, and K. Barton, "Spatial iterative learning control for multi-material three-dimensional structures," *ASME letters in dynamic systems and control*, vol. 1, no. 1, 2021.
- [32] Z. Afkhami, D. J. Hoelzle, and K. Barton, "Robust higher-order spatial iterative learning control for additive manufacturing systems," *IEEE Transactions on Control Systems Technology*, 2023.
- [33] Z. Afkhami, D. Hoelzle, and K. Barton, "Higher-order spatial iterative learning control for additive manufacturing," in *2021 60th IEEE Conference on Decision and Control (CDC)*. IEEE, 2021, pp. 6547–6553.
- [34] Y. Liu and X. Ruan, "Spatial iterative learning control for pitch of wind turbine," in *2018 IEEE 7th Data Driven Control and Learning Systems Conference (DDCLS)*. IEEE, 2018, pp. 841–846.
- [35] L. Yang, Y. Li, D. Huang, J. Xia, and X. Zhou, "Spatial iterative learning control for robotic path learning," *IEEE Transactions on Cybernetics*, 2022.
- [36] Z. Li, C. Yin, H. Ji, and Z. Hou, "Constrained spatial adaptive iterative learning control for trajectory tracking of high speed train," *IEEE Transactions on Intelligent Transportation Systems*, vol. 23, no. 8, pp. 11 720–11 728, 2021.
- [37] Z. Li, Z. Hou, and C. Yin, "Spatial adaptive iterative learning control for automatic driving of high speed train," in *2020 IEEE 9th Data Driven Control and Learning Systems Conference (DDCLS)*. IEEE, 2020, pp. 1440–1445.
- [38] Z. Zhu and X. Zhang, "Spatial adaptive iterative learning control for high-speed train with unknown speed delays," *Proceedings of the Institution of Mechanical Engineers, Part I: Journal of Systems and Control Engineering*, p. 09596518231155960, 2023.
- [39] D. Huang, Y. He, W. Yu, N. Qin, Q. Wang, and P. Sun, "Spatial adaptive iterative learning tracking control for high-speed trains considering passing through neutral sections," *IEEE Transactions on Systems, Man, and Cybernetics: Systems*, 2023.
- [40] Z. Xin and Z. Zijun, "Spatial adaptive iterative learning control based high-speed train operation tracking under external disturbance," *Automatic Control and Computer Sciences*, vol. 57, no. 3, pp. 276–286, 2023.
- [41] B. Kim and S. B. Choi, "Terminal iterative learning control for an electrical powertrain system with backlash," in *2023 IEEE International Conference on Systems, Man, and Cybernetics (SMC)*. IEEE, 2023, pp. 2991–2996.
- [42] D. P. D. Whitworth and M. Harrison, "Tension variations in pliable material in production machinery," *Applied Mathematical Modelling*, vol. 7, no. 3, pp. 189–196, 1983.
- [43] V. G. Papanicolaou, "On the asymptotic stability of a class of linear difference equations," *Mathematics Magazine*, vol. 69, no. 1, pp. 34–43, 1996.

VI. BIOGRAPHY SECTION



production systems.

Zifeng Wang received his B.S degree in mechanical engineering from Shanghai Jiao Tong University in China in 2018. He was a mechanical engineer in Beko China R&D Center from 2018 to 2020. He is currently a Ph.D candidate in Industrial Engineering at Northeastern University, Boston, MA, USA. His research interests include online learning control and data-driven methods in advanced manufacturing processes, aimed at leveraging the repetitiveness and abundant data in manufacturing scenarios to improve the automation and intelligence of industrial



production systems.

Xiaoning Jin (M'12) received the B.S. degree in Industrial Engineering from Shanghai Jiao Tong University, Shanghai, China, in 2006, and the M.S. and Ph.D. degrees in Industrial and Operations Engineering from the University of Michigan, Ann Arbor, MI, USA, in 2008 and 2012, respectively. She was an assistant research scientist in mechanical engineering at the University of Michigan until 2016. She is currently an Associate Professor with the Department of Mechanical and Industrial Engineering at Northeastern University, Boston, MA, USA. Her research interests include intelligent manufacturing systems, data analytics and machine learning, diagnostics and prognostics, and decision support tools.